ISSN 0915-633X

INTERNATIONAL ATOMIC ENERGY AGENCY

THIRTEENTH INTERNATIONAL CONFERENCE ON
PLASMA PHYSICS AND CONTROLLED NUCLEAR FUSION RESEARCH

Washington, DC, United States of America, 1–6 October 1990

IAEA-CN-53/D-3-4

NATIONAL INSTITUTE FOR FUSION SCIENCE

Simulation Study of Nonlinear Dynamics in Reversed-Field Pinch Configuration

K. Kusano, T. Tamano and T. Sato

(Received – Aug. 31, 1990)

NIFS-46 Sep. 1990

RESEARCH REPORT
NIFS Series

NAGOYA, JAPAN

INTERNATIONAL ATOMIC ENERGY AGENCY

THIRTEENTH INTERNATIONAL CONFERENCE ON
PLASMA PHYSICS AND CONTROLLED NUCLEAR FUSION RESEARCH

Washington, DC, United States of America, 1–6 October 1990

IAEA-CN-53/D-3-4

SIMULATION STUDY OF NONLINEAR DYNAMICS IN REVERSED-FIELD PINCH CONFIGURATION

Kanya KUSANO, Teruo TAMANO† and Tetsuya SATO‡

Department of Materials Science, Faculty of Science,
Hiroshima University, Hiroshima 730, Japan
†*General Atomics, San Diego, California 92138-5608, U.S.A.*
‡*National Institute for Fusion Science, Nagoya 464-01, Japan*

keywords: reversed field pinch, dynamo, self-sustainment of reversed field, phase locking, nonlinear dynamics, nonlinear coupling of kink modes, MHD simulation,

SIMULATION STUDY OF NONLINEAR DYNAMICS IN REVERSED-FIELD PINCH CONFIGURATION

Kanya KUSANO, Teruo TAMANO† and Tetsuya SATO‡

Department of Materials Science, Faculty of Science, Hiroshima University, Hiroshima 730, Japan
†*General Atomics, San Diego, California 92138-5608, U.S.A.*
‡*National Institute for Fusion Science, Nagoya 464-01, Japan*

Abstract

Significant progress in our understanding of nonlinear dynamics in reversed-field pinch (RFP) has been achieved through the 3D MHD simulation study. In particular, we have shed light on: 1) the details of the dynamo process, 2) the self-sustainment mechanism, and 3) the phase locking of kink modes. The most important finding in these studies is that the nonlinear coupling between a few unstable kink modes almost plays an essential role in all these MHD dynamics of RFP.

1 Introduction

The key process in the nonlinear dynamics of the reversed field pinch (RFP) is a dynamo action, which has been investigated by many authors. Nevertheless, a lot of questions on the dynamics in the RFP still remain unresolved. In this paper, we consider three subjects concerning the nonlinear dynamics in the RFP. The first is the dynamo process in the RFP. Especially we resolve the question of what is the essential nonlinear coupling in the RFP dynamo process. The second is the self-sustainment, and the third is the phase locking process, which was observed experimentally [1]. Then, we will discuss about the common feature of the nonlinear dynamics in the RFP.

For the investigations of these subjects, we make the best of the magnetohydrodynamic (MHD) simulations, using a Fourier analysis MHD code. In this code, any physical variable $f(r,\theta,z)$ is decomposed into the complex Fourier component $\tilde{f}(r:m;n)$ for the poloidal (m) and the toroidal (n) mode, *i.e.*

$$f(r,\theta,z)=\sum_{m,n}\tilde{f}\,(r:m;n)\exp i(m\theta-nz/R). \tag{1}$$

For the details of this code, one should refer to another paper [2]. The basic equations are the primitive MHD equations, but the density and the plasma pressure are assumed to be homogeneous, $\rho=p=1$. Hence, the pressure driven modes are excluded from the equation system. Actually the focus of our interest is on the nonlinear behaviour of the current driven modes.

We use the boundary condition that guarantees the conservation of the total toroidal magnetic flux and of the total toroidal current. Only for the study of the phase locking process in Section 2.3, however, the perfectly conducting boundary condition is used. The initial condition is always composed of an unstable force-free equilibrium and a perturbation. The equilibrium is specified by the profile of the ratio λ between the magnetic field B and the current J, *i.e.*

$$\lambda=\frac{\mathbf{J}\cdot\mathbf{B}}{\mathrm{B}^2}=\lambda_0\{(\cos\pi r+1)/2\}^{\zeta}. \tag{2}$$

The perturbation is given by the linear eigen-function for the unstable modes.

In the following section (Section 2), the simulation results for three subjects, *dynamo, self-sustainment* and *phase locking* will be shown. In Section 3, we will discuss the general feature of the nonlinear dynamics in the RFP, based on the simulation results.

2 Simulation Results

2.1 Details of the Dynamo Process

Although it is widely believed that the $m = 1$ kink mode instabilities lead to a field reversal process so-called '*dynamo*', the question about the dominant nonlinear coupling in the dynamo process is still in dispute. Roughly speaking, there are two different models of the nonlinear process in the dynamo; the $m = 1$ dynamo and the $m = 0$ dynamo. The former proposes that the coupling of the unstable kink mode with itself is the dominant dynamo coupling [3], while the latter proposes that the $m = 0$ mode driven by the different kink modes generates the dominant dynamo coupling [2,4]. In this subsection, we focus our interest to the question of how large is each contribution of the kink ($m = 1$) mode (linearly unstable) and of the $m = 0$ mode (driven by nonlinear coupling) to the dynamo.

Generally speaking, the dynamo process is a kind of the flux generation process, and hence the dynamo contribution must be evaluated by the amount of the time integration of the dynamo electric field. In the self-reversal process of RFP, it should be given by

$$\Phi^{dynamo}(m; t_0, t_1) = -\int_{t_0}^{t_1} \sum_n \{\tilde{\mathbf{V}}\ (r_{rev}, m, n) \times \tilde{\mathbf{B}}\ (r_{rev}, m, n)\}_\theta dt, \tag{3}$$

where r_{rev} is the radius of the reversal surface. The integration Φ^{dynamo} corresponds to the reversal flux generated by dynamo process for the m mode in the period t_0 to t_1. We carry out four different simulations of the self-reversal process, where four different initial equilibria are employed. These equilibria (IC1, IC2, IC3 and IC4) have the same normalized magnetic helicity (α=6.87; the normalization in α is the same as that in Ref.[5]), but have the different ζ in eq.(2): $\zeta = 0.7$, 0.9, 1.1 and 1.5 for IC1, IC2, IC3 and IC4, respectively. If the total magnetic energy W is normalized by the energy of the Taylor's Bessel-function model state W_{BFM} for $\alpha = 6.87$ [6], the value W/W_{BFM} are 1.059, 1.081, 1.104 and 1.148 for IC1, IC2, IC3 and IC4, respectively. Obviously, the larger ζ leads to the higher magnetic energy. It means that the larger ζ generates the more unstable state for kink modes, since the difference $W - W_{BFM}$ corresponds to an excess magnetic energy driving the MHD instabilities. Figure 1 shows the minus $\Phi^{dynamo}(m; 0, 200\tau_A)$ for $m = 0$ and 1 in the above four simulations. For IC1, the $m = 0$ dynamo flux, $\Phi^{dynamo}(m = 0)$, is larger than the flux for $m = 1$. Hence the contribution from the $m = 0$ mode surpasses that from the $m = 1$ kink mode. As the excess energy is further increased, however, the contribution of the $m = 0$ dynamo gradually decreases as that of the $m = 1$ dynamo increases. For IC4, Φ^{dynamo} for $m = 0$ becomes positive, and hence the $m = 0$ mode acts as an anti-dynamo agency.

These results give an answer to the above question. The contribution of the $m = 0$ mode to the dynamo process depends on the excess energy accumulated in the system just before the dynamo process. The larger the excess energy, the less the contribution of the $m = 0$ mode in comparison with the $m = 1$ mode. Therefore, in order to comprehend more thoroughly the nonlinear dynamics in the RFP experiments, we have to advance to the next question, how large excess energy is spontaneously accumulated in the sustainment phase of the RFP discharge.

2.2 Self-Sustainment Mechanism

Now, we have to find out the dynamo as a spontaneous process in the resistive MHD system, rather than as a result of an instability arising from an initially assumed unstable equilibrium. This requires a numerical simulation of long duration (long compared to the resistive time scale), since the accumulation of the excess energy is due to the resistive evolution in the sustainment phase of the RFP discharge.

Figure 2 shows the long time history of the magnetic energy normalized by W_{BFM} for the two different aspect ratio ((a) 1.6 and (b) 4.8). Figures 3(a) and (b) show the evolution of the radial profile of the toroidal magnetic field, $\mathrm{Re}\{\tilde{B}_z(r, m = n = 0)\}$, for the cases. We can clearly see in Fig.2(a) that the magnetic energy has an oscillation that is composed of the slow ramp-up phase and the fast relaxation phase like a sawtooth oscillation. The slow ramp is due to the resistive evolution, while the fast relaxation is due to the dynamo. Figure 3(a) shows that at each relaxation phase the reversed field is spontaneously generated and the value B_z on the axis and the wall decreases sharply. It is worth noting that the critical level of the excess energy, at which the dynamo process starts, is fixed at about 6% of W_{BFM}. On the other hand, in Figs. 2(b) and 3(b) we can find that the critical excess energy and the oscillation amplitude in the large aspect ratio case are about one percent smaller than those in the small aspect ratio case. These results indicate that the critical excess energy and the amplitude of the energy oscillation depend on the aspect ratio of the device.

In order to explain physically the dependence on the aspect ratio, we analyze the linear stability for ideal kink modes of the $(m;n)$=(0;0) component before and after the typical dynamo process, which starts at $270\tau_A$ in the small aspect ratio case. Table I shows the linear growth rate for the most unstable two kink modes $(m;n) = (1;3)$ and (1;4) at four different times, where the symbol '-' means that the mode is stable at that time. The growth rate of the mode (1;3) gradually increases with time. Just before the relaxation process starts ($t = 256\tau_A$) the adjacent mode (1;4) becomes unstable in addition to (1;3). After the relaxation process ends, however, both modes become stable again ($t = 300\tau_A$). This result is consistent with the $m = 0$ dynamo model, in which at least two kink modes must be unstable to drive nonlinearly the m=0 mode. So, we can explain the reason why the critical energy depends on the aspect ratio, using the $m = 0$ dynamo model. The interval between the neighboring kink modes in wavelength space,

$$\Delta\lambda \equiv \lambda_n - \lambda_{n+1} = \lambda_n^2(2\pi R + \lambda_n)^{-1},$$

is larger as the aspect ratio R becomes smaller, where $\lambda_n = 2\pi R/n$. The larger $\Delta\lambda$ requires the wider unstable region and also the higher excess energy.

Now we can conclude that the RFP configuration is sustained in a cyclic process, where the MHD relaxation (dynamo) phase and the resistive diffusion phase appear cyclically and alternatively. When at least two kink ($m = 1$) modes become ideally unstable, MHD relaxation can take place. This is due to the fact that the MHD relaxation progresses through the dynamo process for the $m = 0$ mode. The larger the aspect ratio of the device, the lower the critical excess energy for the dynamo and the smaller the amplitude of the oscillation. Remember that the critical energy even for the small aspect ratio (1.6) is at most 6% of W_{BFM}. This value is lower than the excess energy of the initial equilibrium IC2 in the previous subsection. As expected from this result, the dynamo flux for the $m = 0$ mode is actually confirmed to be as large as that for the $m = 1$ mode. Therefore, as long as the aspect ratio is as large as those in the usual experimental devices, the critical excess energy can not be higher than about 6% of the Taylor's minimum energy. Namely, it is impossible for the $m = 1$ dynamo to overpower the $m = 0$ dynamo. Through the detailed examination, we have further found some other characteristics of this relaxation-diffusion oscillation (see Ref.[2]).

The dependence of the oscillation on the aspect ratio gives an interpretation for the different behaviour of the experimental plasmas between the large aspect ratio and the small aspect ratio devices. In the small aspect ratio device like MST, the clear sawtooth oscillation is always observed, while in the large aspect ratio device like ZT-40M it is observed only for the high θ discharge [7,8]. Our result suggests that the oscillation is always present even in the large aspect ratio device, but that the amplitude of the oscillation becomes as small as the level of background fluctuation for the low θ discharge.

2.3 Phase Locking of Kink Modes

Phase locking of kink modes is numerically observed in the simulations of self-reversal and self-sustainment processes. It has characteristics similar to the 'slinky mode' observed in the OHTE experiment [1]: 1) It appears when the MHD relaxation process occurs. 2) Only for the resonant modes does phase locking occur. Figure 4 shows the typical results of the phase locking, where the normalized toroidal profiles for $\mathrm{Re}\{\tilde{B}_r(r=0.9, m=1, z)\}$ are plotted for the internal kink modes ($n = 11$ to 20) at three different times. In this simulation, the initial perturbation $\mathbf{v}_0$ and $\mathbf{b}_0$ incorporates seven different kink modes ($n = 2$ to 9), *i.e.*

$$\begin{pmatrix} \mathbf{v}_0 \\ \mathbf{b}_0 \end{pmatrix} = \sum_{n=2}^{9} \begin{pmatrix} \tilde{\mathbf{v}}_{eigen-function}(r,n) \\ \tilde{\mathbf{b}}_{eigen-function}(r,n) \end{pmatrix} \exp i(\theta - nz/R + \phi_n), \tag{4}$$

where the original phase distribution ϕ_n is given by a random number. Figure 4(a) shows that the phase distribution is completely random at $t = 10\tau_A$. It is owing to the initial random phase distribution for the unstable modes. At $t = 28\tau_A$, however, the phases of these internal kink modes are locked at a certain toroidal location where $z = 1.1$ (Fig.4(b)). After then the phase locking is lost and the phase distribution becomes random again (Fig.4(c)).

Now, let us consider a question of what determines the toroidal location where the phase locking takes place. Figure 5 shows the relation between two toroidal locations $z_{p.l.}$ and $z_{4/5}$ for the 27 different simulations, those have different phase distributions $\{\phi_n\}$ in eq.(4). The location $z_{p.l.}$ is where the phase locking takes place, but the location z_{n_1/n_2} is the location where the two kink modes, $(m;n) = (1,n_1)$ and $(1,n_2)$, initially have the same phase, *i.e.*

$$z_{n_1/n_2} = R\frac{\phi_{n_1} - \phi_{n_2}}{n_1 - n_2}. \tag{5}$$

We can see that there is a good correlation between the locations $z_{p.l.}$ and $z_{4/5}$. However, for the other modes except (1;4) and (1;5) we can not observe a correlation with the $z_{p.l.}$. In fact, the modes (1;4) and (1;5) are the most unstable modes in the initial perturbation. These results mean that the most dominant two kink modes rule the other modes through the nonlinear coupling between them, and introduce the phase locking. We also confirm that if the most dominant mode (1;5) is excluded from the system, the phase locking process becomes more obscure.

It is worthwhile to point out that in these simulations the perfectly conducting boundary condition is adopted. Therefore, the phase locking process is not a special phenomena of the RFP with a resistive shell, but is a general characteristic in the MHD relaxation processes. This result is consistent with the other simulation study [9].

3 Discussion

Through the simulation study presented, we can conclude that the fundamental mechanism in the RFP dynamics is a coherent process rather than a turbulent one. Namely, the dynamo, that is a

key agent for the nonlinear dynamics in the RFP, is led by the nonlinear coupling between a few (almost only two) kink modes unstable ideally. Of course, the RFP plasma is a turbulent plasma that usually has a broad Fourier wave spectrum and a large stochastic region of the magnetic field lines of force. However, at least in the MHD regime, these two phenomenological characteristics of a turbulent plasma in the RFP are merely the effects of the nonlinear coupling in a dynamo process.

References

[1] T.Tamano, W.D.Bard, C.Chu, Y.Kondoh, R.J.L.Haye, P.S.Lee, M.Saito, M.J.Schaffer, and P.L.Taylor. *Phys. Rev. Lett.*, **59** (1987) 1444.

[2] K.Kusano and T.Sato. *Nuclear Fusion*, **30** No. 10 or 11 (1990) (to appear).

[3] R.A.Nebel, E.J.Caramana, and D.D.Schnack. *Phys. Fluids B*, 1 (1989) 1671.

[4] K.Kusano and T.Sato. *Nuclear Fusion*, **27** (1987) 821.

[5] A.Reiman. *Phys. Fluids*, **23** (1980) 230.

[6] J.B.Taylor. *Phys. Rev. Lett.*, **33** (1974) 1139.

[7] R.B.Howell, J.L.Ingraham, G.A.Wurden, P.G.Weber, and C.J.Buchenauer. *Phys. Fluids*, **30** (1987) 1828.

[8] S.Prager. In Proc. *U.S.-Japan Workshop on Numerical Simulation of Reversed-Field Pinches, (Jan. 16-18, 1989, San Diego, hosted by Science Applications International Corporation, San Diego, CA 92121) Internal Rep. SAIC-90/1165.*

[9] D.D.Schnack and S.Ortolani. *Nuclear Fusion*, **30** 1990.

Table I: Instantaneous growth rate (τ_A^{-1}) of the ideal kink instability for the most unstable two kink modes in the case of the small aspect ratio.

n	$t = 152\tau_A$	$t = 200\tau_A$	$t = 256\tau_A$	$t = 300\tau_A$
3	1.1×10^{-1}	2.7×10^{-1}	2.9×10^{-1}	-
4	-	-	1.6×10^{-3}	-

Figure Caption

FIG. 1. The dynamo flux, $\Phi^{dynamo}(m, 0, 200\tau_A)$ in the simulations using IC1, IC2, IC3 and IC4. The open circles are for $m = 0$, and the solid circles are for $m = 1$.

FIG. 2. Time history of the total magnetic energy W in the cases of (a) the small aspect ratio (1.6) and of (b) the large aspect ratio (4.8). The energy is normalized by a Taylor's minimum energy W_{BFM} that is determined from the instantaneous α.

FIG. 3. Time history of $B_z - r$ profile for (a) the small and (b) the large aspect ratio.

FIG. 4. The normalized mode profile of $\mathrm{Re}\{\tilde{B}_r(r = 0.9 : m = 1; n)\exp(-inz)\}$ for $n = 11$ to 20 at three different times ((a) $t = 10\tau_A$, (b) 28 τ_A, and (c) 40 τ_A).

FIG. 5. The phase locking points $z_{p.l.}$ are plotted as a function of the location $z_{4/5}$ where the modes $(m; n) = (1;4)$ and $(1;5)$ initially have a same phase. The solid circles show the 27 different simulation results, in which the different phase distribution in the initial perturbation is adopted, respectively.

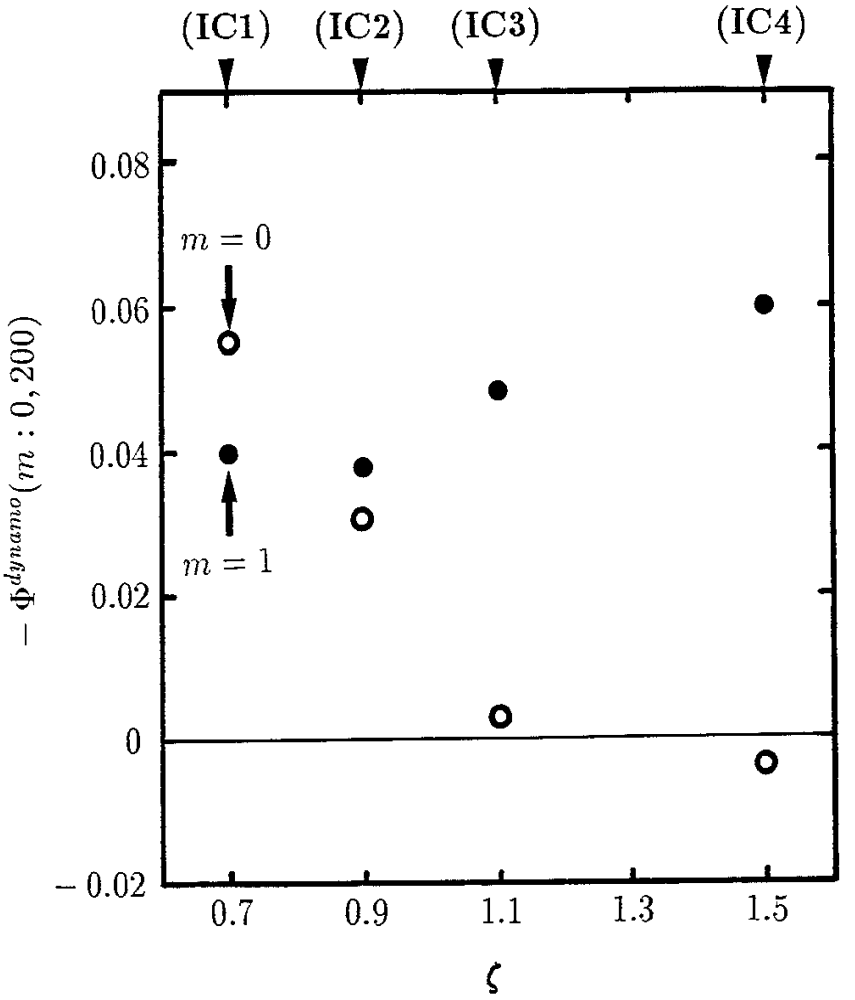
(IC1)
(IC2)
(IC3)
(IC4)
0.08
0.06
0.04
0.02
0
− 0.02
$m = 0$
$m = 1$
$-\Phi^{dynamo}(m:0,200)$
0.7
0.9
1.1
1.3
1.5
ζ

Fig.1

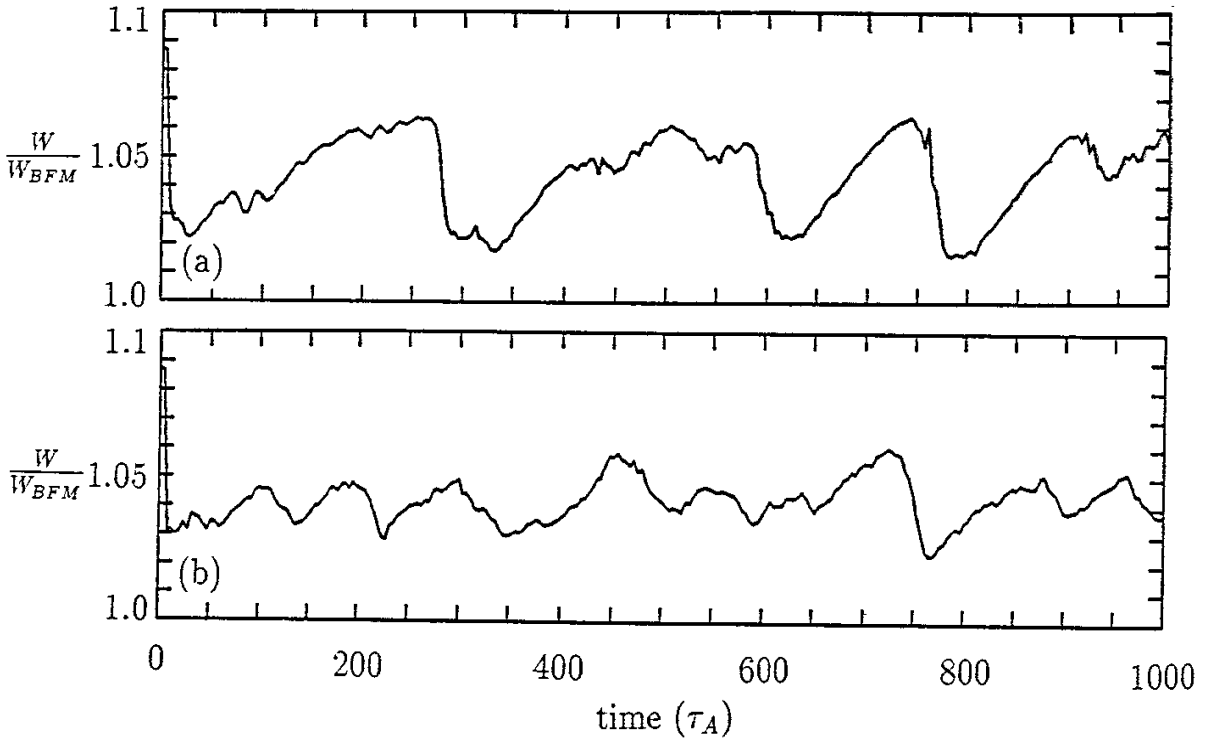
1.1
$\frac{W}{W_{BFM}}$ 1.05
1.0
(a)
1.1
$\frac{W}{W_{BFM}}$ 1.05
1.0
(b)
0
200
400
600
800
1000
time (τ_A)

Fig.2

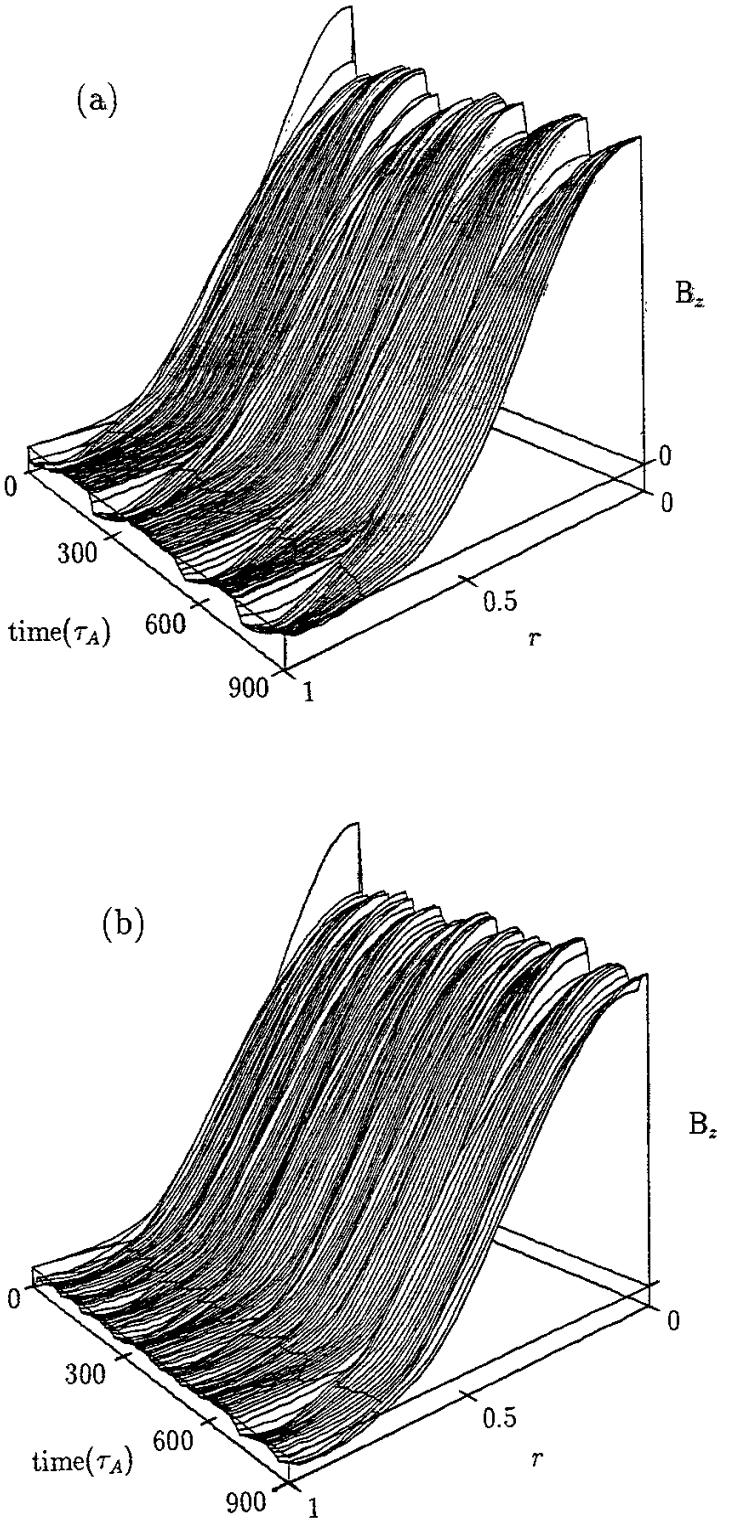
(a)
B_z
0
0
0
300
time(τ_A)
600
900
0.5
r
1
(b)
B_z
0
0
300
time(τ_A)
600
900
0.5
r
1

Fig.3

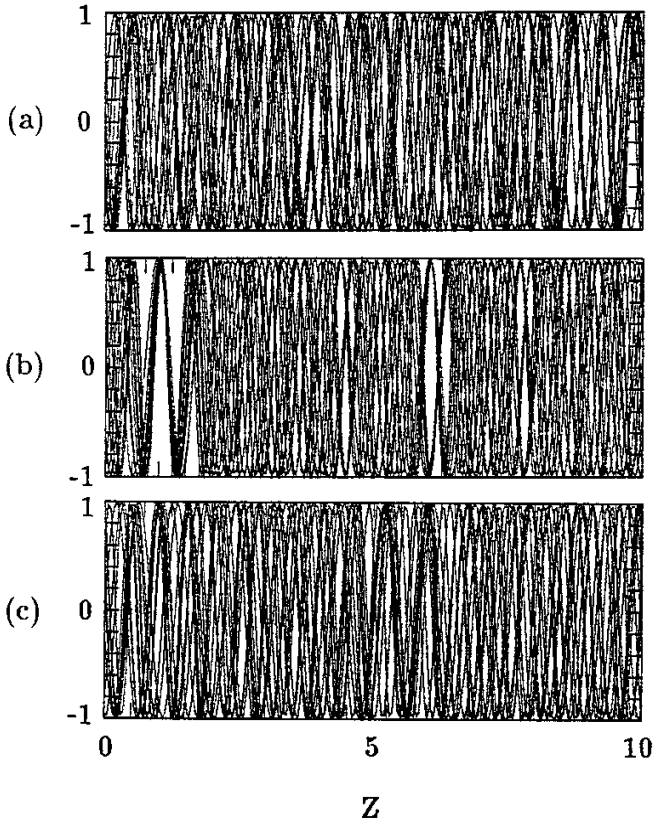

Fig.4

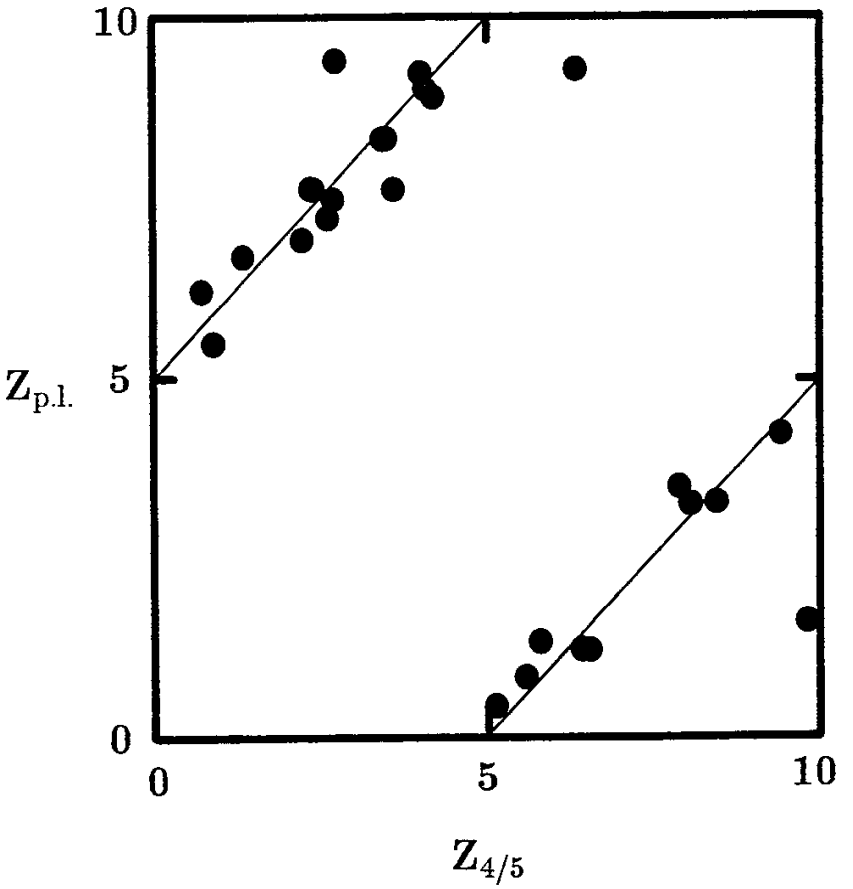

Fig.5